# Structural characterization, third-order nonlinear optical properties and Hirshfeld surface analysis of bis(dimethylammonium) hexachlorostannate(IV)

RM. Sockalingam[1*], C. Balakrishnan[1], M. Manonmani[1]
[1]Department of Chemistry, Annamalai University, Annamalainagar
Tamilnadu – 608 002, India

***Abstract:*** Bis(dimethylammonium) hexachlorostannate(IV) (DMAHCS) crystals were grown by slow evaporation solution growth technique. The characteristic functional groups present in the molecules are confirmed by FT-IR analysis and the crystallinity is confirmed by powder XRD analysis. Single crystal X-ray diffraction analysis showed that the $Sn^{4+}$ ion being surrounded by six chloride anions in a distorted octahedral geometry. A diffuse reflectance spectrum (DRS) illustrated intense charge transfer in the compound. The observed band gap value for the compound is 4.17 eV estimated using the Kubelka-Munk function. Nonlinear optical absorption of the sample has been studied at 532 nm using single 5 ns laser pulses, employing the open and closed -aperture Z-scan technique. Investigation of the intermolecular interactions and crystal packing using Hirshfeld surface analysis, derived by single crystal XRD data, reveals the close contacts associated with strong interactions.

***Keywords*- X-ray diffraction, Band gap, Z-scan technique, Hirshfeld surface analysis.**

## 1. INTRODUCTION

The search for novel nonlinear optical (NLO) crystals is gaining increased attention in recent years, especially the researches on inorganic-organic hybrid compounds are attracting much attentions because of their unique optoelectronic [1], switchable nonlinear optical and luminescent properties [2,3], photoelectric and ferroelectric properties [4], solar cells [5] and light-emitting devices [6]. Recently, Crystal structure of bis(4-methylpyridinium) hexachlorotin(IV) [7], bis(1-phenylethylammonium) hexachloridostannate(IV) and bis(2-phenylethylammonium) hexachloridostannate(IV) [8], bis (phenylammonium) hexachlorotin(IV) [9], bis(4-acetylanilinium) hexachloridostannate(IV) [10] tetrakis(4-bromoanilinium) hexachlorotin(IV)dichloride [11], bis(4-methylanilinium) hexachlorostannate(IV) monohydrate [12] 3,3′-diammoniumdiphenylsulfone hexachloridostannate monohydrate [13] tetrakis(anilinium) hexachlorotin(IV) dichloride [14], bis(guanidinium) hexachlorostannate(IV) [15], bis(2-chloroethyl) ammonium hexachlorostannate [16] and 4-chloropyridinium hexachlorostannate(IV) [17] have been reported.

In the present investigation, we report the structural characterization, optical and third-order nonlinear optical responses of the title compound. Computational studies were used to investigate dipolemoment, polarizability and first-order molecular hyperpolarizability. Molecular interactions are quantified by finger print plots derived from Hirshfeld surfaces.

## 2. EXPERIMENTAL

### 2.1 Preparation of dimethylammonium hexachlorostannate(IV)

Dimethylformamide (0.2 mL, 2mM) and hydrochloric acid (2 mL) in ether were mixed at room temperature to obtain dimethylammonium hydrochloride precursor solution. Tin chloride was prepared by dissolving tin shots (0.118g, 1mM) in 5mL hydrochloric acid at room temperature (7 hours). To the freshly prepared ethanolic solution of dimethylammonium hydrochloride precursor solution, tin chloride was added with constant stirring. Crystallization took place in 14-16 d and the crystals were harvested. Optical and scanning electron microscope images of the as-grown DMAHCS crystals are shown in Fig. 1 and the chemical reaction is given as.

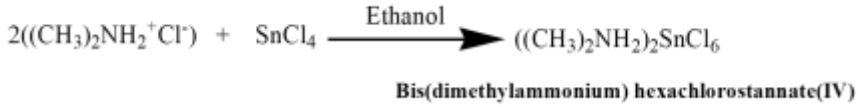


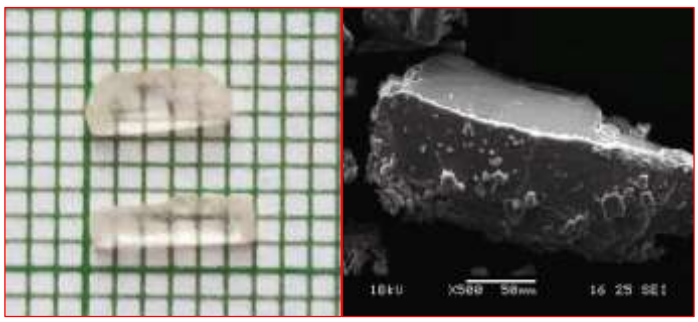

**Figure 1.** Optical and SEM images of DMAHCS

### 2.2 Characterization techniques

The FT-IR spectrum was recorded using a CARY 630 FT-IR instrument in the range of 400–4000 $cm^{-1}$. A Bruker AXS (Kappa Apex II) X-ray diffractometer was used for single crystal XRD studies. The powder X-ray diffraction was performed by using Philips Xpert pro triple-axis X-ray diffractometer at room temperature at a wavelength of 1.540˚A with a step size of 0.008º. The samples were examined with CuKα radiation in the 2θ range of 10–50º. The surface morphologies of the sample were observed using a JEOLSM 5610 LV SEM with the resolution of 3.0 nm, an acceleration voltage range of 0.3–20 kV. The UV–DRS spectra was recorded using Shimadzu UV2600 UV-Vis spectrophotometer. Photoluminescence spectra was recorded by LS55 Fluorescence spectrometer.

### 2.3 Computational studies

Polarizability, hyperpolarizability and dipolemoment were performed using the GAUSSIAN 09W [18] program using density functional group theory (DFT) B3LYP method with LanL2DZ as the basis set. Hirshfeld surfaces and fingerprint plots were generated from the crystal data using the CrystalExplorer (Version 3.1) [19-22], using DFT method with 6-31G (d,p) as basis set. Simulated XRD patterns derived from Mercury 3.6 program.

## 3. Results and discussion

### 3.1 FT-IR

The functional groups are identified by FT-IR spectrum in the spectral range of 400–4000 $cm^{-1}$ (Fig. 2). The broad band observed at 3394 $cm^{-1}$ corresponds to the asymmetric stretching vibration of $NH_2$ group and symmetric stretching vibration was observed at 3186$cm^{-1}$ [23]. The N-H bending vibration is observed at 1572 $cm^{-1}$. The medium intensity band at 1389 $cm^{-1}$ is due to the stretching vibration of C-N moiety [24]. An absorption band in the region 2800 – 3000 $cm^{-1}$ is due to aliphatic C-H stretching frequency.

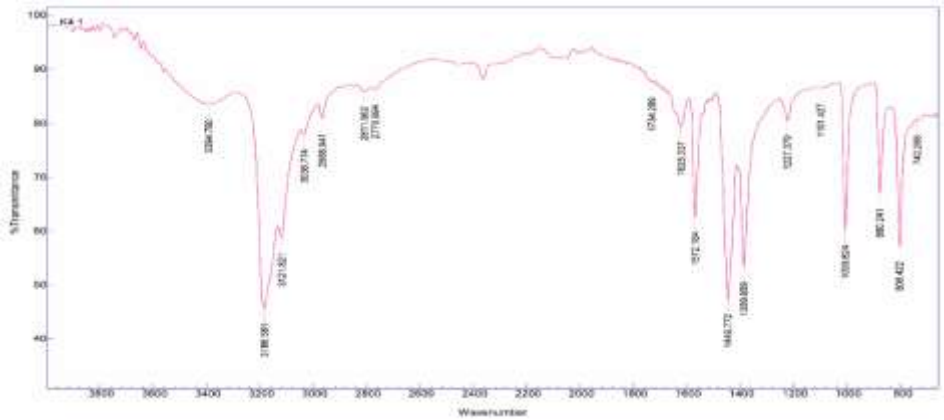

**Figure 2.** FT-IR spectrum of DMAHCS

### 3.2 Powder XRD analysis

The powder XRD pattern of DMAHCS shows that the sample is of single phase without detectable impurity. The well-defined Bragg's peaks at specific 2θ angles show the good crystallinity of the material. Peak positions in the powder XRD patterns matche with simulated single crystal XRD pattern, derived from Mercury 3.6 program. High intensity sharp peaks show good crystalline nature of the complex (Fig. 3).

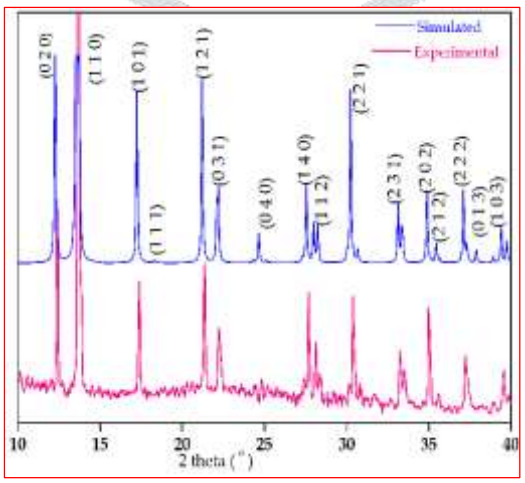


**Figure 3.** XRD Patterns of DMAHCS

### 3.3 Single crystal XRD

The structure of DMAHCS was elucidated by single crystal X-ray diffraction analysis. The compound crystallizes in the orthorhombic crystal system with centrosymmetric space group P*nnm*. Crystal data and structure refinement parameters are listed

in Table 1. The cell parameters are in agreement with already reported values [25]. Table 2 summarizes the bond angles and lengths. The ORTEP and optimized molecular structure of the DMAHCS is illustrated in Fig. 4. Dimethylammonium hexachlorostannate(IV) contains the tin ion in a distorted octahedral environment of six chloride ions. The Sn-Cl interatomic distances vary from 2.4198(15) to 2.429(2) Å. The molecule shows extensive hydrogen bonding as shown in Table 3. Hydrogen bonding has a clear effect on increasing the hyperpolarizability value, resulting in enhanced NLO activity because of facile charge transfer.

Table 1. Crystal data and structure refinement for DMAHCS

| Crystal Data | **DMAHCS** | |
|---|---|---|
| Empirical formula | $C_4H_{16}Cl_6N_2Sn$ | |
| Formula weight | 423.58 | |
| Temperature | 296(2) K | |
| Wavelength | 0.71073 Å | |
| Crystal system | Orthorhombic | |
| Space group | P*nnm* | |
| Unit cell dimensions | a = 7.3225(5) Å | α= 90°. |
| | b = 14.4260(11) Å | β= 90° |
| | c = 7.2165(5) Å | γ = 90° |
| Volume | 762.31(9) $Å^3$ | |
| Z | 2 | |
| Density (calculated) | 1.845 Mg/m3 | |
| Absorption coefficient | 2.695 mm-1 | |
| F(000) | 412 | |
| Crystal size | 0.150 x 0.150 x 0.100 mm3 | |
| Theta range for data collection | 3.965 to 24.993°. | |
| Index ranges | -8<=h<=8, -17<=k<=17, -8<=l<=8 | |
| Reflections collected | 6867 | |
| Independent reflections | 730 [R(int) = 0.0787] | |
| Completeness to theta =24.993° | 99.30% | |
| Absorption correction | Semi-empirical from equivalents | |
| Max. and min. transmission | 0.7452 and 0.5468 | |
| Refinement method | Full-matrix least-squares on $F^2$ | |
| Data / restraints / parameters | 730 / 0 / 40 | |
| Goodness-of-fit on $F^2$ | 1.219 | |
| Final R indices [I>2sigma(I)] | R1 = 0.0500, wR2 = 0.1409 | |
| R indices (all data) | R1 = 0.0566, wR2 = 0.1521 | |
| Extinction coefficient | n/a | |
| Largest diff. peak and hole | 1.445 and -1.307 e.$Å^{-3}$ | |
| CCDC | **1886213** | |

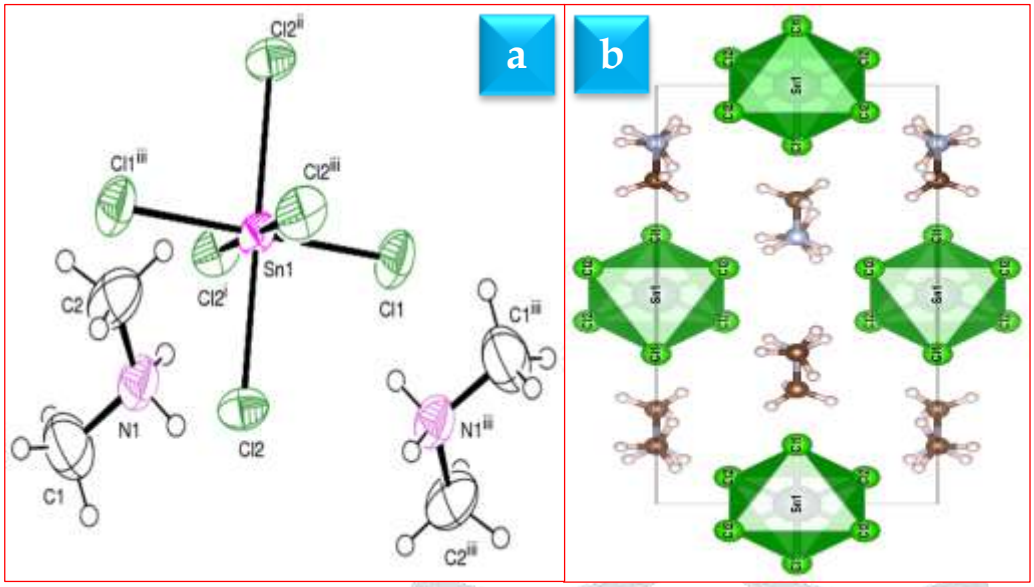


**Figure 4.** (a)ORTEP and (b) packing diagram of DMAHCS

Table 2. Bond lengths [Å] and angles [°] for DMAHCS

| Bond lengths [Å] | | | |
|---|---|---|---|
| C(1)-N(1) | 1.455(14) | N(1)-H(1D) | 0.890 |
| C(1)-H(1A) | 0.960 | N(1)-H(1E) | 0.890 |
| C(1)-H(1B) | 0.960 | Cl(1)-Sn(1) | 2.429(2) |
| C(1)-H(1C) | 0.960 | Cl(2)-Sn(1) | 2.4198(15) |
| C(2)-N(1) | 1.442(13) | Sn(1)-Cl(2)#1 | 2.4198(16) |
| C(2)-H(2A) | 0.960 | Sn(1)-Cl(2)#2 | 2.4198(16) |
| C(2)-H(2B) | 0.960 | Sn(1)-Cl(2)#3 | 2.4198(16) |
| C(2)-H(2C) | 0.960 | Sn(1)-Cl(1)#2 | 2.429(2) |
| Bond Angles [°] | | | |
| N(1)-C(1)-H(1A) | 109.50 | C(1)-N(1)-H(1E) | 108.1 |
| N(1)-C(1)-H(1B) | 109.50 | H(1D)-N(1)-H(1E) | 107.3 |
| H(1A)-C(1)-H(1B) | 109.50 | Cl(2)-Sn(1)-Cl(2)#1 | 88.08(8) |
| N(1)-C(1)-H(1C) | 109.50 | Cl(2)-Sn(1)-Cl(2)#2 | 180 |
| H(1A)-C(1)-H(1C) | 109.50 | Cl(2)#1-Sn(1)-Cl(2)#2 | 91.92(8) |
| H(1B)-C(1)-H(1C) | 109.50 | Cl(2)-Sn(1)-Cl(2)#3 | 91.92(8) |
| N(1)-C(2)-H(2A) | 109.50 | Cl(2)#1-Sn(1)-Cl(2)#3 | 180 |
| N(1)-C(2)-H(2B) | 109.50 | Cl(2)#2-Sn(1)-Cl(2)#3 | 88.08(8) |
| H(2A)-C(2)-H(2B) | 109.50 | Cl(2)-Sn(1)-Cl(1) | 89.61(7) |
| N(1)-C(2)-H(2C) | 109.50 | Cl(2)#1-Sn(1)-Cl(1) | 90.39(7) |
| H(2A)-C(2)-H(2C) | 109.50 | Cl(2)#2-Sn(1)-Cl(1) | 90.39(7) |
| H(2B)-C(2)-H(2C) | 109.50 | Cl(2)#3-Sn(1)-Cl(1) | 89.61(7) |
| C(2)-N(1)-C(1) | 116.9(10) | Cl(2)-Sn(1)-Cl(1)#2 | 90.39(7) |
| C(2)-N(1)-H(1D) | 108.1 | Cl(2)#1-Sn(1)-Cl(1)#2 | 89.61(7) |
| C(1)-N(1)-H(1D) | 108.1 | Cl(2)#2-Sn(1)-Cl(1)#2 | 89.61(7) |
| C(2)-N(1)-H(1E) | 108.1 | Cl(2)#3-Sn(1)-Cl(1)#2 | 90.39(7) |
| | | Cl(1)-Sn(1)-Cl(1)#2 | 180 |

Symmetry transformations used to generate equivalent atoms:
#1 -x,-y+1,z #2 -x,-y+1,-z #3 x,y,-z

Table 3. Hydrogen bonds for DMFHCS [Å and °]

| D-H···A | d(D-H) | d(H···A) | d(D···A) | <(DHA) |
|---|---|---|---|---|
| C(2)-H(2A)····Cl(2) | 0.96 | 2.91 | 3.812(11) | 157.1 |
| C(2)-H(2C)···· Cl(1) | 0.96 | 2.96 | 3.619(13) | 126.8 |
| N(1)-H(1D)···· Cl(1) | 0.89 | 2.94 | 3.6097(4) | 133.1 |
| N(1)-H(1D)···· Cl(2) | 0.89 | 2.84 | 3.530(7) | 135.0 |
| N(1)-H(1D)···· Cl(2) | 0.89 | 2.72 | 3.454(6) | 139.9 |
| N(1)-H(1E)···· Cl(1) | 0.89 | 2.94 | 3.6097(4) | 133.1 |
| N(1)-H(1E)···· Cl(2) | 0.89 | 2.72 | 3.454(6) | 139.9 |

| | | | | |
|---|---|---|---|---|
| N(1)-H(1E)··· Cl(2) | 0.89 | 2.84 | 3.530(7) | 135.0 |

Symmetry transformations used to generate equivalent atoms:

### 3.4 Optical studies

Diffuse reflectance spectrum of DMAHCS is shown in Fig. 5a. The cut-off wave length is observed at ~285. The band gap was determined to be 4.14 eV using a plot of $(F(R)hv)^2$ *versus* hv, where F(R), Kubelka-Munk function [26].

On excitation of DMAHCS with 285 nm radiation, the compound exhibited emission band as shown in Fig. 5b. The maximum appeared at 401 nm. Relatively low full width half maximum (FWHM) associated with the band indicates better quality of epilayers present [27].

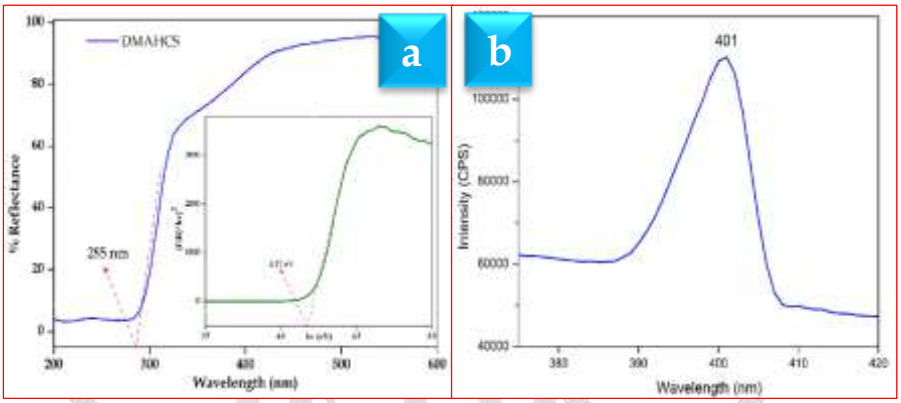


**Figure 5** (a) UV- vis spectrum (Tauc plot is given as an inset) (b) Photoluminescence emission spectrum in the solid state at room temperature

### 3.5 Z-scan studies

The Z-scan method is a simple method for determining nonlinear absorption and refractive index [28]. Studies are carried out using Q-switched Nd:YAG laser having 5 ns pulses at a repletion rate of 10 Hz giving second harmonic at 532 nm. It is based on the principle of spatial beam distortion. The transmittance changes through a small aperture at the far field position (closed aperture) can determine the amplitude of the phase shift (Δφ). Further, by moving the sample through the focus without placing an aperture at the detector (open aperture), the intensity dependent absorption of the sample is measured. The open aperture Z-scan transmittance is insensitive to the nonlinear refraction and effective only for the nonlinear absorption while the closed aperture transmittance is sensitive to investigate both nonlinear absorption and nonlinear refraction [29]. Fig. 6 shows the recorded closed and open aperture normalized transmittance curves of DMAHCS. Close agreement between experimental and theoretical data suggests the third order character of NLO effect.

The nonlinear refractive index ($n_2$) was estimated by using the following equation [30]

$$n_2 = \frac{\Delta\Phi_0}{KI_0L_{eff}} \quad (1)$$

where K is wave vector ($K= 2\pi/\lambda$) and $I_0$ is the intensity of the laser beam at the focal point ($I_o = 6.29 \times 10^9$ W/cm$^2$) and $\Delta\phi_o$ is the on-axis phase shift. The nonlinear absorption coefficient ($\beta$) can be estimated from the open aperture technique using the standard relation [31] given by

$$\beta = \frac{2\sqrt{2}\Delta T}{I_0L_{eff}} \quad (2)$$

where ΔT is minimum transmittance value at the open aperture Z-scan curve. Values of $n_2$ and $\beta$ can be used to calculate the real [Re($\chi^{(3)}$)] and imaginary parts [Im($\chi^{(3)}$)] of the third-order nonlinear optical susceptibility, ($\chi^{(3)}$). The absolute value of $\chi^{(3)}$ can be calculated by the following relation [32]

$$|\chi^{(3)}| = \left[\left(\mathrm{Re}(\chi^{(3)})\right)^2 + \left(\mathrm{Im}(\chi^{(3)})\right)^2\right]^{1/2} \quad (3)$$

The pre-focal transmittance minimum (valley) followed by a post-focal transmittance maximum (peak) obtained from the closed aperture Z-scan method indicates that the sign of the nonlinear refractive index is positive ($n_2>>0$) exhibiting self-focusing effect [33]. In the open aperture method decrease in transmittance near the focus and positive sign of nonlinear absorption (β) are suggestive of the reverse saturated absorption (RSA). Table 4 lists the experimental results of the third-order nonlinear optical parameters of DMAHCS. The $\chi^{(3)}$ values of some of the good NLO materials such as potassium dihydrogen phosphate (KDP) and deuterated potassium dihydrogen phosphate (DKDP) are, 8.34 x $10^{-14}$, 6.51 x $10^{-14}$ esu respectively [34]. Comparison reveals that this material has a good third-order NLO response.

Table 4. Calculated third-order nonlinear optical parameters from Z- scan experimental data

| Third-order NLO properties | Calculated values |
|---|---|
| β ×$10^{-12}$ (m/W) | 7.0346 |
| $n_2$ × $10^{-19}$(m$^2$/W) | 5.8165 |
| $R_e\chi^{(3)}$ × $10^{-13}$ (esu) | 1.8638 |

| | |
|---|---|
| $I_m\chi^{(3)} \times 10^{-13}$ (esu) | 0.9548 |
| $\chi^{(3)} \times 10^{-13}$ (esu) | 2.0941 |
| Optical limiting (J cm$^{-2}$) | 20.46 |

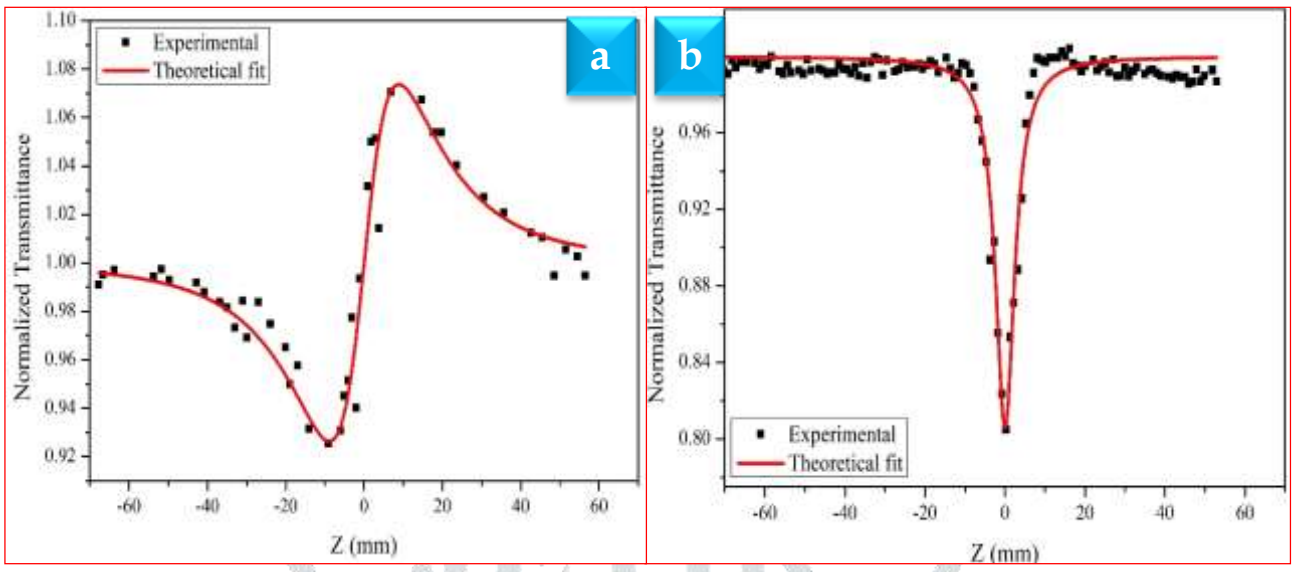


**Figure 6.** a) Closed aperture curve b) Open aperture curve

### 3.6 Optical limiting behaviour

DMAHCS prefers centrosymmetric space group P*nnm* and as a result second-order optical nonlinearity vanishes [35]. For Gaussian beam, input fluence (dividing fluence with the pulse width of the laser gives the intensity) varies with position 'z' and it is given as

$$E(z) = {}^{4\sqrt{\ln 2}E_{in}}\Big/_{\pi^{3/2}\,\omega(z)^2} \qquad (4)$$

where ω(z) is the beam radius and $E_{in}$ is the input beam energy [36]. No change in transmittance is observed at low input fluencies obeying Beer's law. The transmittance decreases markedly as irradiance fluence exceeded 20.46 J cm$^{-2}$. Nonlinear behaviour is a typical characteristic of optical limiting phenomena [37]. Two photon absorption mechanism [38] could be the possible reason for the observed nonlinear absorption and hence optical limiting effect. Theoretical fit of this mechanism based on Z-scan theory gives the best fit for experimental data. Also, Z-scan open aperture curve, Fig. 6b exhibits minimum transmittance in the focus at valley suggesting the possibility of reverse saturable absorption (RSA) mechanism [39].

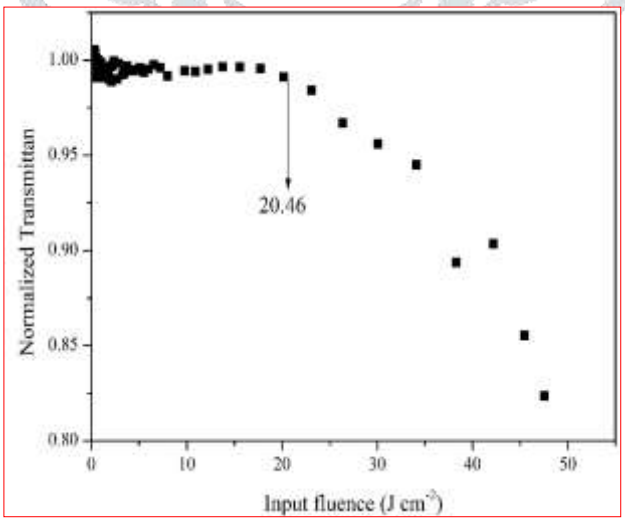


**Figure 7.** The optical limiting response of DMAHCS

### 3.7 First-order molecular hyperpolarizability

The NLO response of DMAHCS at the molecular level is also confirmed by computational studies, and the calculated dipole moment (μ), polarizability (α) and first-order molecular hyperpolarizability (β) of the specimen are 13.7434 D, 76.8143 x 10$^{-24}$ esu and 1.5524 x 10$^{-30}$ esu (~8 times that of urea), respectively (Table 5). Observed micro level nonlinear response could be due to strong inter- and intramolecular hydrogen bonding interaction enhancing the hyperpolarizability.

Table 5. The calculated dipole moment (in D), β components (a.u.), $\beta_{tot}$ value (in esu), and α components (a.u.), $\alpha_{tot}$ value (in esu)

| First-order molecular hyperpolarizability | | Polarizability | |
|---|---|---|---|
| $\beta_{xxx}$ | 3.4076 | $\alpha_{xx}$ | 63.8516 |
| $\beta_{xxy}$ | 134.9230 | $\alpha_{xy}$ | 85.2379 |
| $\beta_{xyy}$ | 4.1773 | $\alpha_{yy}$ | 21.3863 |
| $\beta_{yyy}$ | 39.5304 | $\alpha_{xz}$ | 0.0005 |
| $\beta_{xxz}$ | 8.3074 | $\alpha_{yz}$ | 0.1153 |
| $\beta_{xyz}$ | 4.9779 | $\alpha_{zz}$ | 0.0467 |
| $\beta_{yyz}$ | -1.7897 | **$\alpha_{tot}$ (x $10^{-24}$) esu** | **76.8143** |
| $\beta_{xzz}$ | -5.9053 | **Dipole moment (D)** | |
| $\beta_{yzz}$ | 5.0572 | $\mu_x$ | -0.0454 |
| $\beta_{zzz}$ | 1.2591 | $\mu_y$ | 13.7381 |
| **$\beta_{total}$ (x $10^{-30}$) esu** | **1.5524** | $\mu_z$ | 0.3760 |
| | | $\mu$ | **13.7434** |

### 3.8 Hirshfeld surface analysis

Hirshfeld surfaces and fingerprint plots were generated by crystal explorer program. The normalized contact distances $d_{norm}$ is based on $d_e$ and $d_i$ representing the distances of the nearest nucleus external and internal to the surface respectively. The shape index indicates the shape of the electron density surface around the molecular interactions. The visible deep red circular depressions indicate hydrogen bonding contacts (Fig. 8(a-c)). Whereas the visible bright red area in $d_e$ plot of Fig. 8(b) indicating Cl···H dominant interactions. The small light colour range area represents the weaker and longer contacts excluding the hydrogen bonds.

Molecular interactions are quantified by fingerprint plots as shown in Fig. 9. A spike in the lower right area represents Cl···H (40.1%) interactions whereas left region represents the H···Cl (28.9%) interactions. The middle and tail part of the fingerprint plot indicates H···H (28.2%) and Cl···Cl (2.7%) respectively.

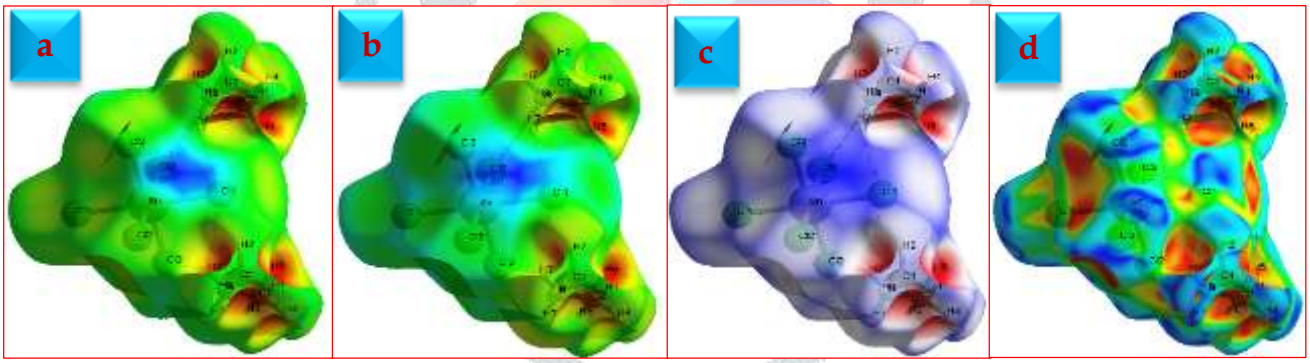


**Figure 8** Hirshfeld surface of DMAHCS (a) $d_e$ (b) $d_i$ (c)$d_{norm}$ and (d) shape index

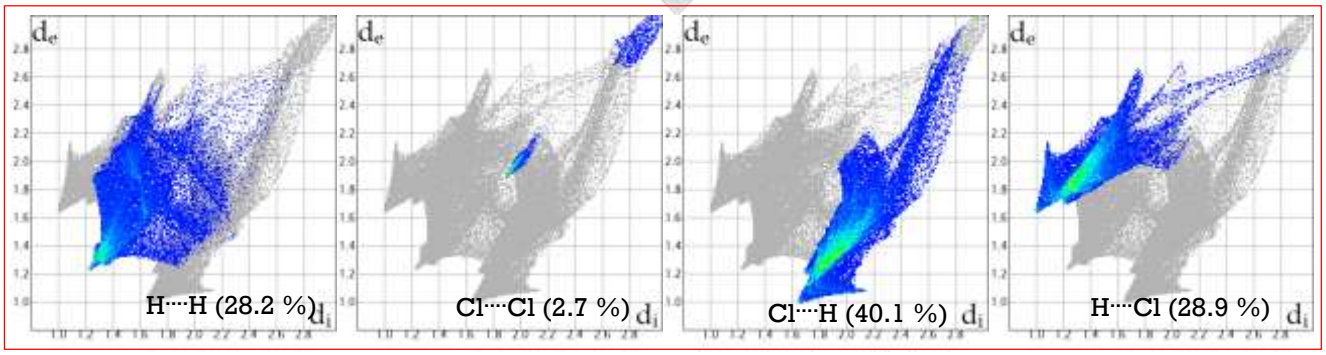


**Figure 9** Fingerprint plots of DMAHCS

### 4. Conclusion

Single crystals of dimethylammonium hexachlorostannate(IV) are grown by slow evaporation solution growth technique and characterized by XRD analysis, SEM, FT-IR, UV-DRS and photo-luminescence emission spectrum. Hydrogen bonding

interactions enhance the hyperpolarizability leading to significant the NLO activities. The good third-order NLO responses indicate that the title complex qualifies as a good optical material.

**References**


[1] J. S. Manser, J. A. Christians and Prashant V. Kamat, "Intriguing Optoelectronic Properties of Metal Halide Perovskites", *Chem. Rev.*, 116, 12956−13008, 2016.

[2] Lin Zhou, Xuan Zheng, Ping-Ping Shi, Zainab Zafar, Heng-Yun Ye, Da-Wei Fu and Qiong Ye, "Switchable Nonlinear Optical and Tunable Luminescent Properties Triggered by Multiple Phase Transitions in a Perovskite-Like Compound", *Inorg. Chem.*, 56, 3238−3244, 2017.

[3] C. C. Stoumpos, C. D. Malliakas and M. G. Kanatzidis, "Semiconducting Tin and Lead Iodide Perovskites with Organic Cations: Phase Transitions, High Mobilities, and Near-Infrared Photoluminescent Properties", *Inorg. Chem.,* 52(15), 9019–9038, 2013.

[4] Xitao Liu, Peiqing Long, Zhihua Sun and Zhiguo Yi, "Optical, Electrical and Photoelectric Properties of Layered perovskite Ferroelectric $Bi_2WO_6$ Crystals", *J. Mater. Chem.* C, 6, 00, 1-7, 2016.

[5] F. Hao, C. C. Stoumpos, D. H. Cao, R. P. H. Chang and M. G. Kanatzidis, "Lead-free solid-state organic–inorganic halide perovskite solar cells", *Nature Photonics*, 8(6), 489–494, 2014.

[6] L. Lanzetta, J. M. Marin-Beloqui, I. Sanchez-Molina, D. Ding and S. A. Haque, "Two-Dimensional Organic Tin Two-Dimensional Organic Tin Halide Perovskites with Tunable Visible Emission and Their Use in Light-Emitting Devices", *ACS Energy Lett.* 2, 1662−1668, 2017.

[7] Z. Liu, H. Dai, J. Fan, W. Yu, X. Tao and M. Jiang, "Crystal structure of bis(4-methylpyridinium) hexachlorotin(IV), $(C_6H_8N)_2SnCl_6$. *Z. Kristallogr. NCS*, 224, 79-80, 2009.

[8] D. G. Billing, A, Lemmerer and M. Rademeyer, "Bis(1-phenylethylammonium) hexachloridostannate(IV) and bis(2-phenylethylammonium) hexachloridostannate(IV)". *Acta Cryst.* C63, m101–m104, 2007.

[9] S. Karoui and S. Kamoun, "Crystal Structure, Vibrational and Electrical Properties of the Bis (phenylammonium) Hexachlorotin(IV): $(C_6H_5NH_3)_2$*$SnCl_6$", *International Journal of Science and Research*, 4(10), 2201-2210, 2015.

[10] X.-W. Song, R.-T. Xue, S.-G. Chen and Y.-S. Yin, Bis(4-acetylanilinium) hexachloridostannate(IV). *Acta Cryst.* E67, m653–m653, 2011.

[11] Zhi Liu, Hong-Xia Dai, Dan Zhao, Wen-Tao Yu, De-Liang Cui, Xu-Tang Tao and Min-Hua Jiang, "Crystal structure of tetrakis(4-bromoanilinium) hexachlorotin(IV) dichloride, $(BrC_6H_4NH_3)_4[SnCl_6]Cl_2$", *Z. Kristallogr. NCS*, 225, 389-390, 2010.

[12] S. BelhajSalah, M. S. M. Abdelbaky, S. García-Granda, K. Essalah, C. Ben Nasr and M. L. Mrad, Crystal structure, Hirshfeld surfaces computational study and physicochemical characterization of the hybrid material $(C_7H_{10}N)_2[SnCl_6].H_2O$. *J. Mol. Struct.*, 1152, 276–286, 2018.

[13] A. Kessentini, T. Dammak and M. Belhouchet, "Synthesis, molecular structure, vibrational spectroscopy, optical investigation and DFT study of a novel hybrid material: 3,3′-diammoniumdiphenylsulfone hexachloridostannate monohydrate". *J. Mol. Struct.*, 1149, 818–827, 2017.

[14] M. Rademeyer, "Tetrakis(anilinium) hexachlorotin(IV) dichloride", *Acta Cryst.* E60(3), m345–m347, 2004.

[15] H. Ishida, Y. Furukawa and S.Kashino, "Bis(guanidiniurn) hexachlorostannate(IV)", *Acta Cryst.*, C55, 1995-1997, 1999.

[16] C. J. Kane, R. Long, W. E. Pettit, G. L. Breneman, and G. R. Pettit, Structure of bis(2-chloroethyl)ammonium hexachlorostannate. *Acta Cryst.*, 48(8), 1490–1491, 1992.

[17] R. C. Gearhart, T. B. Brill, W. A. Welsh, and R. H. Wood, "Crystal Structure of 4-Chloropyridinium Hexachlorostannate(IV)", *J. Chem. Soc., Dalton Trans.*, 4, 359-361, 1973.

[18] Frisch, M. J., & Trucks, G. W., et al. (2009). Gaussian09, Revision C.01, Gaussian, Inc., Wallingford, CT.

[19] M. A. Spackman and D. Jayatilaka, *CrystEngComm.*, 11, 19-32, 2009.

[20] F. L. Hirshfeld, *Theoret. Chim. Acta.*, 44, 129-138, 1977.

[21] CrystalExplorer (Version 3.1), S. K. Wolff, D. J. Grimwood, J. J. McKinnon, M. J. Turner, D. Jayatilaka and M. A. Spackman, University of Western Australia, 2012.

[22] M. A. Spackman and J. J. McKinnon, *CrystEngComm.*, 4, 378-392, 2002.

[23] L. shepard Gray Jr, "Characteristic infrared absorption frequencies of nitrogen-containing bonds", digital repository@lowa state university, 1958.

[24] C. W. M. Yuen, S. K. A. Ku, P. S. R. Choi, C. W. Kan and S. Y. Tsang, "Determining Functional Groups of Commercially Available Ink-Jet Printing Reactive Dyes Using Infrared Spectroscopy" *RJTA*, 9, 26, 2005.

[25] M. H. Ben Ghozlen, A. Daoud and J. W. Bats, "Dimethylammonium Hexaehlorostannate(IV)", *Acta Cryst.*, B37, 1415-1416, 1981.

[26] P. Kubelka and F. Munk, Ein Beitrag zur Optik der Farbanstriche, *Z. Tech. Phys.*, 12, 593-601, 1931.

[27] Chun-Yi Sun, Xin-Long Wang, Xiao Zhang, Chao Qin, Peng Li, Zhong-Min Su , Dong-Xia Zhu, Guo-Gang Shan, Kui-Zhan Shao, Han Wu and Jing Li, "Efficient and tunable white-light emission of metal–organic frameworks by iridium-complex encapsulation", *Nat. Commun.*, 4, 1-8, 2013.

[28] R. Signorini, R. Bozio and M. Prato, "Optical Limiting Applications", *Springer*, 295-326, 2002.

[29] M. Sheik-Bahae, A. A. Said, T. H. Wei, D. J. Hagan and E. W. Van Stryland, "Sensitive measurement of optical nonlinearities using a single beam", IEEE *J. Quant. Electron.*, 26, 760-769, 1990.

[30] T. Kanagasekaran, P. Mythili, P. Srinivasan, A. Y. Nooraldeen, P. K. Palanisamy, R. Gopalakrishnan, "Studies on the Growth, Optical, Thermal, and Mechanical Properties of Pure and o-Nitroaniline Doped Benzil Crystals", *J. Cryst. Growth Des.*, **8** 2335-2339, 2008.

[31] M. Sheik-Bahae, A. A. Said, E.W. Van Stryland, "High-sensitivity, single-beam $n_2$ measurements", *Opt. Lett.*, 14, 955-957, 1989.
[32] P. Sathy, R. Philip, V.P.N. Nampoori, C.P.G. Vallaban, "Photoacoustic observation of excited singlet state absorption in the laser dye rhodamine 6G", *J. Phys*., D27, 2019-2022, 1994.
[33] M. C. Sreenath, S. Mathew, I. Hubert Joe, V. K. Rastogi, "Z-scan measurements of the third-order optical nonlinearities and vibrational spectral studies by DFT computations on azo dye 1-(2-Methylphenylazo)-2-napthol", *Optics and Laser Technology*, 97, 390-399, 2017.
[34] D. Wang, T. Li, S. Wang, J. Wang, Z. Wang, X. Xu, F. Zhang, "Study on nonlinear refractive properties of KDP and DKDP crystals", *RSC Adv*. 6, 14490-14495, 2016.
[35] H. R. Manjunath, "Growth, characterization, crystal and molecular structure studies of 1-(2' -thiophen)-3-(2,3,5-trichlorophenyl)-2-propen-1-one", *J. Cryst. Growth.,* 327, 161-166, 2011.
[36] Z. Sun, G. Zhang, X. Wang, Z. Gao, X. Cheng, S. Zhang, D. Xu, "Growth, Morphology, Thermal, Spectral, Linear, and Nonlinear Optical Properties of l-Arginine Bis(trifluoroacetate) Crystal", *Cryst. Growth Des*., 9, 3251-3259, 2009.
[37] H. I. Elim, J. Yang, J. Y. Lee, J. Mi, W. Ji, ""Observation of saturable and reverse-saturable absorption at longitudinal surface plasmon resonance in gold nanorods", *Appl. Phys. Lett.,* 88, 083107 1-3, 2006.
[38] G. S He, L. S. Tan, Q. Zheng, P. N. Prasad, "Multiphoton Absorbing Materials: Molecular Designs, Characterizations, and Applications", *Chem. Rev.*,108, 1245-1330, 2008.
[39] L. Polavarapu, Q. H. Xu, M. S. Dhoni, W. Ji, "Optical limiting properties of silver nanoprisms", *Appl. Phys. Lett.,* 92, 263110 1-3, 2008.